# Hierarchical Structure of Magnetic Nanoparticles -$Fe_3O_4$- Ferrofluids Revealed by Small Angle X-Ray Scattering

**Gea Fitria[1], Arum Patriati[2], Mujamilah[2], Maria Christina Prihatiningsih[1], Edy Giri Rachman Putra[1,2*], and Siriwat Soontaranon[3]**

[1]*Department of Nuclear Chemical Engineering, Polytechnic Institute of Nuclear Technology, Indonesia, Jl. Babarsari, Yogyakarta 55281, Indonesia*

[2]*Center for Science and Technology of Advanced Materials, National Nuclear Energy Agency of Indonesia, Kawasan Puspiptek Serpong, Banten 15314, Indonesia*

[3]*Synchrotron Light Research Institute of Thailand, 111 University Avenue, Nakhon Ratchasima 30000, Thailand*

* ***Corresponding author:***

*email: giri@batan.go.id*

*Received: August 28, 2020*
*Accepted: November 20, 2020*

**DOI:** 10.22146/ijc.59114

***Abstract:*** *Small-angle X-ray scattering (SAXS) experiments were set up to investigate the form and structure of $Fe_3O_4$ magnetic nanoparticles (MNPs) using BL1.3:SAXS at the Synchrotron Light Research Institute (SLRI) of Thailand in the range of scattering vector q, $0.7 < q\ (nm^{-1}) < 4$. The scattering data from samples, background, and empty cells were collected and then subtracted using small-angle X-ray scattering image tool (SAXSIT) software. The analysis of the corrected scattering patterns for four different pH, i.e., 2, 3, 4, and 5, has been revealed by applying log-normal spherical and mass fractal models calculation. The results showed that the SAXS measurement could investigate the hierarchical structures of MNPs $Fe_3O_4$ containing primary and secondary particles. The two-dimensional fractal ($D_f$) aggregates as secondary particles (in volume) have various sizes ranging from 21 to 103 nm in diameter, confirming the correlation to their pH. Those structures consist of primary particles with a mean length of 2 nm in radius and the particle size distribution (σ) of 0.5.*

***Keywords:*** *magnetic nanoparticles $Fe_3O_4$; ferrofluids; small-angle scattering; X-ray synchrotron; nanostructures; hierarchical structure*

## ■ INTRODUCTION

Ferrofluids are highly stable colloidal systems containing magnetic nanoparticles (MNPs) $Fe_3O_4$, which can be physically controlled using external magnetic fields. The study of ferrofluids has progressed in recent years due to many possible applications in the biomedical field. As described in a review paper by Wu et al., magnetic nanoparticles have been used for medical applications such as drug delivery agents, biosensing, and bioseparation [1]. However, due to the magnetic properties of MNPs $Fe_3O_4$, they tend to form clusters or aggregate in volume. The presence of aggregates and their internal structure will strongly influence the properties of MNPs. For example, the number of primary particles forming aggregate can affect the strength of magnetic interaction. The larger aggregate with more primary particles and interaction with each of them will result in strong magnetic properties [2]. Usually, the surface of magnetic nanoparticles is altered to prevent interparticle surface interactions [3].

As a fundamental understanding, the importance of the aggregation and the properties of the hierarchical structure of MNPs $Fe_3O_4$ becomes a crucial matter that must be explored further due to its effects on magnetic properties and applications. Rodriquez et al. [4] and Sulungbudi et al. [5] have measured magnetic nanoparticles' structure using dynamic light scattering (DLS) and transmission electron microscopy (TEM). By comparing the size that was measured using DLS and TEM, they pointed out that the particles formed

aggregates. However, in the case of aggregate structures, both of the measurements simply give the information about the overall size of aggregates and could not provide the information about the size of each primary particles that formed aggregate to reveal its hierarchical structure. Therefore, it is necessary to employ the other techniques that could show the hierarchical structure of MNPs $Fe_3O_4$ to obtain a deep understanding of the aggregation mechanism.

Small-angle scattering (SAS), including X-ray (SAXS) and neutron (SANS), is a powerful technique to investigate size disorders of material structures, ranging from 1 to 100 nm. Detailed information of the nanostructures such as aggregate phenomena, fractal structure, and dimensions of MNPs $Fe_3O_4$ as well as its hierarchical structures can be obtained through this technique [6-7].

Previously, the study of fractal aggregates of MNPs using the small-angle scattering technique has been undertaken by many researchers. Taufiq et al. [8] and Putra et al. [9] reported the measurement of MNPs $Fe_3O_4$ using small-angle neutron scattering (SANS). They pointed out by using two model combinations that the hierarchical structure could be measured. In this case, SAS measurement's vital process is how to cultivate and acquire the valuable information from scattering data that is usually carried out through fitting analysis. However, the two previous works still briefly explain the detailed analysis, including each step for the analysis process and the meaning for each obtained parameter.

In this work, a series of MNPs $Fe_3O_4$ was prepared via co-precipitation method as a pH function and then characterized using SAXS instrument. The established data analysis was applied to cultivate the scattering data to understand better and explain aggregation phenomena, fractal structure, and hierarchy structure.

## ■ EXPERIMENTAL SECTION

### Sample Preparation

Magnetic nanoparticles (MPNs) $Fe_3O_4$ were synthesized by co-precipitation method at Center for Science and Technology of Advanced Materials, BATAN-Indonesia. A detailed explanation about the synthesis process has been published in previous work [5]. The SAXS measurement was carried out at room temperature using a liquid cell with an aperture of 4 × 10 mm and thickness of 1.5 mm for each sample. The samples' concentration was 1 mg/mL with different pH conditions, i.e. 2, 3, 4, and 5.

### Small Angle X-ray Scattering (SAXS) Measurement

The SAXS experiments were performed at BL 1.3: SAXS at SLRI, Thailand. A 2-dimensional charge-coupled device (CCD, Rayonix SX165, LX170HS) detector with a diameter of 165 mm was put 1.5 m and 4.5 m away from the sample. The 1.5 m and 4.5 m setups provided $q$ range of $0.07 < q\ (nm^{-1}) < 0.4$ with $q = (4\pi/\lambda) \sin \theta$, where $\theta$ is the scattering angle, and $\lambda$ is the wavelength of the incident beam.

Scattering intensities of each sample were subtracted from the empty cell and the solvent backgrounds (pure $H_2O$) using data reduction software, SAXSIT [10]. The corrected scattering intensity data were normalized and then fitted with a combination of two models calculation, log-normal spherical and mass fractal models using data analysis software, SASfit [11].

### Data Analysis

#### *Data import*

**Analyze standard.** Analyze Standard using SAXSIT software is carried out for calibration of SAXS measurement called q-range calibration using silver behenate crystal as a standard. The crystal has several peaks that give the same d-spacing structure of 5.838 nm. There are two parameters needed to determine i.e., sample detector distance (SDD) or L and the distance between the direct beam and scattering ring or D to calibrate the q-range [10].

**Data reduction.** The 2-dimensional scattering intensities were normalized using the background substraction process to reduce the cell's scattering effect and the solvent backgrounds during experiments. Afterward, the scattering profile is calculated to radially averaged from the 2-dimensional pattern to q into the 1-dimensional pattern, consisting of two parameters, intensity I(q) and scattering vector q. While the intensity is obtained from the measurement, the scattering vector

is resulted from the calculation using parameters D and L, the distance between the direct beam to scattering ring, and sample detector distance (SDD), respectively, through q-calibration, Eq. (1),

$$2\theta = \tan^{-1}\left(\frac{D}{L}\right) \quad (1)$$

Then, the scattering vector (q) is found from Eq. (2) [12],

$$q = \frac{4\pi}{\lambda}\sin\theta \quad (2)$$

### *Model fitting*

The main aim of the SASfit program is to adjust the fitting model calculation to the scattering pattern of the sample. The fitting process is carried out to obtain the high suitability between the intensity of the $I_{mod}(q)$ or theoretical and the intensity of the $I_{exp}(q)$ or experiment.

The scattering intensity I(q) from all samples as a function of scattering vector was calculated using Eq. (3),

$$I(q) \approx S(q) \cdot P(q) \quad (3)$$

where S(q) is the structure factor that, in this case, explains the aggregate structures, and P(q) is the form factor that explains the size and shape of primary particles. The simplest form model, the sphere, was used to investigate particle morphology. In contrast, a log-normal distribution model was applied due to the MNP's tendency to form aggregate and had broad distribution. Hence, a log-normal spherical model as a form factor calculation, which is a good approximation to start the calculation, was applied to fit the experimental data. The scattering function for the sphere particle with radius r is calculated with the Eq. (4),

$$P(q) = \phi V_p^2 \Delta\rho^2 F(qr_0)^2 f(r) \quad (4)$$

where P(q) is form factor, $\phi$ is volume fraction, $\Delta\rho$ is scattering length density difference. With the particle volume $(V_p) = (4/3)\,\pi r_0^3$, the spherical form factor is given by,

$$F(qr_0) = \frac{3[\sin(qr_0) - qr_0\cos(qr_0)]}{(qR)^3} \quad (5)$$

The term of f(r) in Eq. (4) could be explained with the Eq. (6),

$$f(r) = \frac{N}{C_{LN}}\frac{1}{r^p}\exp\left(\frac{1}{2\sigma^2}(\ln r - \ln r_{med})^2\right) \quad (6)$$

Where

$$C_{LN} = \sqrt{2\pi} r_{med}^{1-p} \exp\left((1-p)^2\frac{\sigma^2}{2}\right) \quad (7)$$

In the global fitting, besides the log-normal spherical model, the fractal model as structure factor was also applied to explain the interaction between the MNPs or, in this case, called fractal aggregate. Therefore, the scattering intensity can be expressed as [13],

$$I(q) = \int N(r_0)F^2(qr_0)dr_0 S(q,\xi,D_f,r_0) \quad (8)$$

where N, $F(q,r_0)$ and $S(q, \xi, D_f, r_0)$ are the number density of the particles, the scattering amplitude, and the structure factor. The characteristics of the structure factor of the samples are given in the following equation,

$$S(q) = 1 + \frac{D_f\Gamma(D_f - 1)}{(qr_0)^{D_f}\left[1 + 1/(q^2\xi)^2\right]^{(D_f-1)/2}} \times \sin\left[(D_f - 1)\tan^{-1}(q\xi)\right] \quad (9)$$

where $\Gamma$ is the gamma function, $D_f$ is the fractal dimensions, and $\xi$ is correlation length or the size of fractal an aggregate.

The best fit corresponds to the minimum residuum and chi-square values. These values show the difference between theoretical calculation and experimental fits, which are the fit parameters' estimates. The best-fitting results can be seen from the residuum not oscillating, and the data spread evenly. This indicates that there is high suitability between the model calculation and experimental data.

## ■ RESULTS AND DISCUSSION

The corrected scattering intensity data were obtained by subtraction of each raw data sample using the SAXSIT program. The process was carried out to subtract the scattering intensities to get scattering from particles only, see Fig. 1(a).

Furthermore, Fig. 1(b) shows the final result of the data reduction process where a 1-dimensional plot is radially averaged intensity as a function of scattering vector q from the 2-dimensional pattern. Thus, this pattern will be used for further analysis using SASfit.

According to Fig. 2, the scattering pattern at the first region at large-q values shows the characteristic of the interference between the scattering object and the

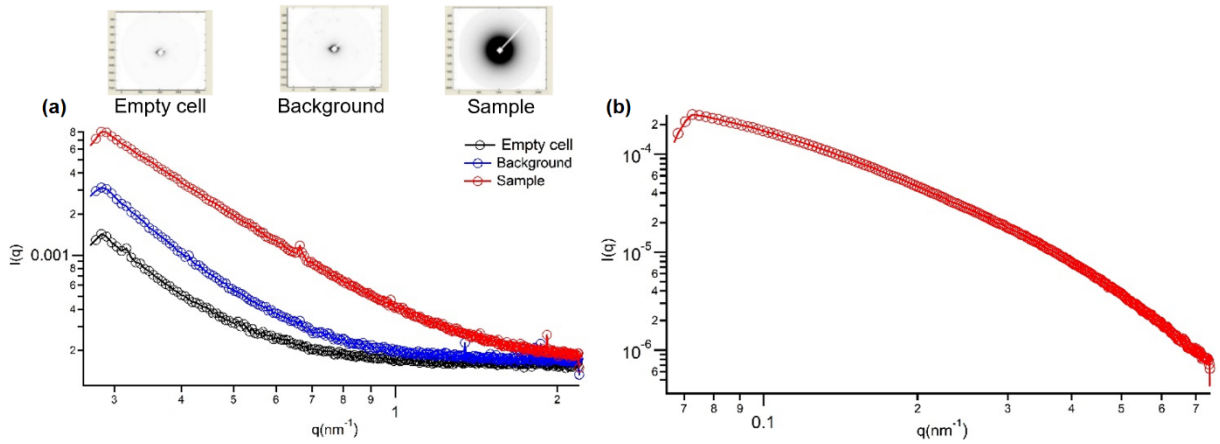


**Fig 1.** (a) Small-angle scattering pattern of the three measurements (2-dimensional and 1-dimensional patterns), namely empty cell, background, and sample (b) The corrected 1-dimensional scattering pattern

solvent. This region is called the Porod zone, which means that the primary particles' scattering intensity decreases following a power law of $I(q) \sim q^4$. In this region, the scattering pattern is started at the high to intermediate *q* region as $S(q) \approx 1$. Then the size of the primary particles and polydispersity of the primary particles can be determined. The existence of particles with broad size distribution can be confirmed by the absence of an oscillatory behavior on the scattering curve.

The second region in Fig. 2 defined for intermediate to the low-*q* range with the data as $I(q) \approx S(q)$. The nonlinearity at the low-q range can be caused by the interference effects with the neighboring particles. The slope in the low *q* range appeared, indicating the particles' aggregation effect, and the Guiner behavior does not occur. This effect makes larger particles that are measured by the SAXS technique. This showed that many spherical particles as primary particles formed aggregates or fractal objects as secondary particles. In this region, the scattering intensity falls, following a power law of $I(q) \sim q^{D_f}$ and the size of aggregate can be determined [12]. The correlation of particles formed aggregate within the system occurred due to the large surface and the magnetic forces and the ionic force.

Both of the two regions are fitted separately with a combination of two models calculation to obtain the best fitting results and parameters fitting in the two regions. These two models are determined based on the direct

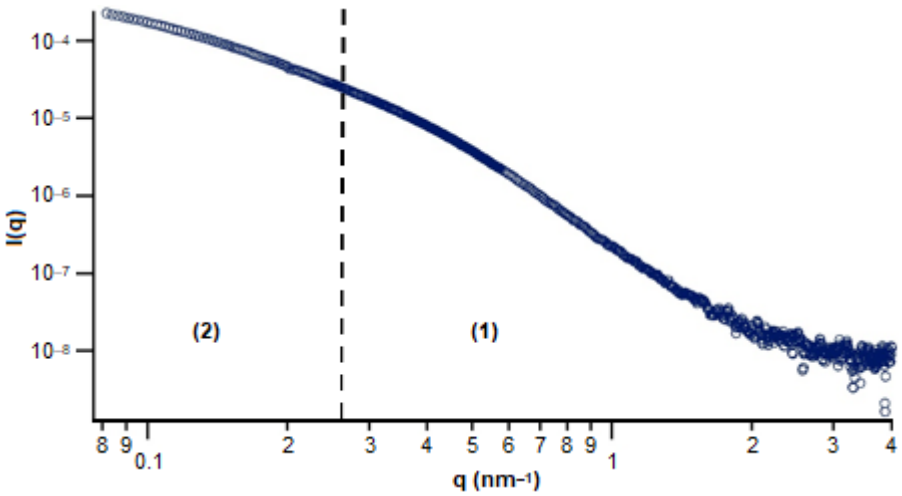


**Fig 2.** Different phenomenon is measured based on scattering pattern (1) First region at high-q values (2) Second region at low-q values

analysis of scattering patterns and literature such as previous papers to acquire the initial assumptions about the MNPs. Moreover, other techniques such as dynamic light scattering (DLS) were also applied to make initial assumptions and ensure the fitting results.

The first assumption that can be applied through model fitting is correlated particles to get the suitable structural information. Fig. 3(a) shows the fitting process by following the log-normal sphere model calculation for the first region. According to the fitting process result, a mean primary radius is 2 nm with the polydispersity 0.5. Fig. 3(b) shows the fitting process's result through the mass fractal model calculation for the second region, and the primary particles were assumed in a spherical shape and monodisperse. The size of fractal objects or aggregates is about 21 nm to 103 nm as the variation of pH.

Fig. 4 shows the scattering pattern in all samples' log-log plot; the black dash line shows that the scattering is close to $q^{-2}$ behavior as a slope -2 in agreement at low q region or $q < 0.03$ nm$^{-1}$. This means that the fractal objects had a two-dimensional structure in the range of $1.9 \leq D_f \leq 2.1$.

The combination of two theoretical models resulted in the best-fitted data and also proved that Porod law (high to intermediate q range) and power-law scattering (intermediate to low q range) are appearing for all the pH variation. With increasing the pH, the existence of primary particles and aggregates are always detected. From the fitting results through the mass fractal model, the size of aggregates is 21 nm, 24 nm, 33 nm, and 103 nm in diameter for the pH of 2, 3, 4, and 5, respectively.

The results from DLS measurement that confirmed SAXS measurement are hydrodynamic diameter ($d_H$) as the overall diameter of MNPs $Fe_3O_4$ aggregates, see Table 1.

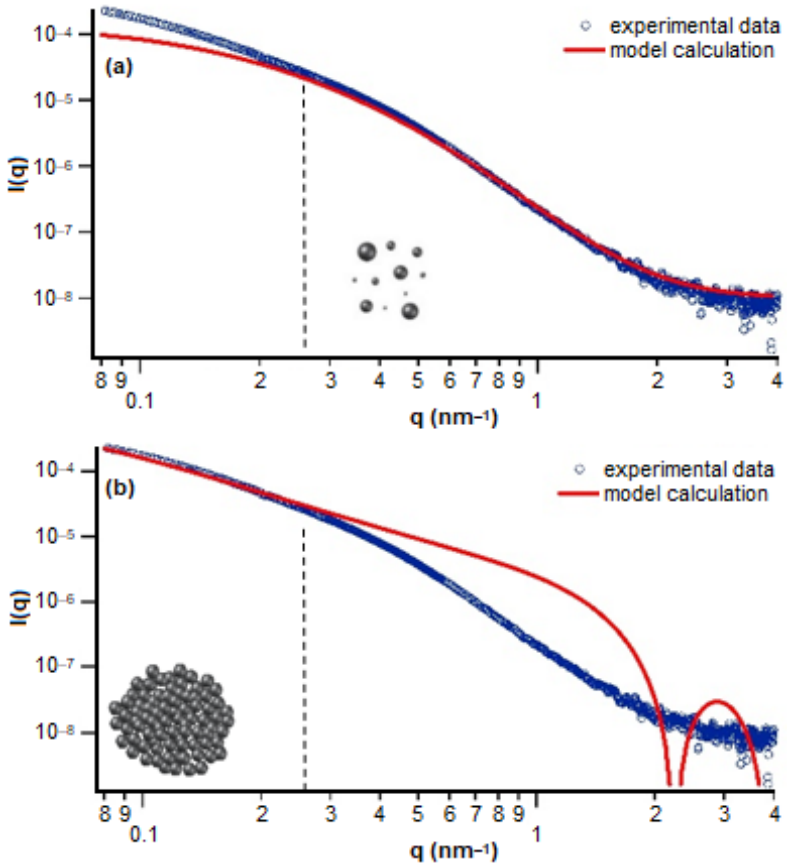


**Fig 3.** Fitting process of SAXS profiles of ferrofluid sample fitted with two model calculations (a) log-normal sphere model at high to intermediate q region and (b) mass fractal model at intermediate to low q region

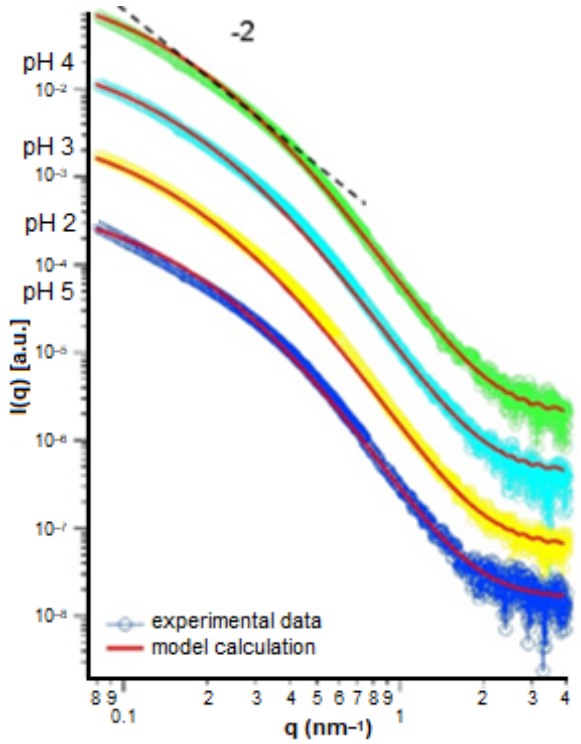


**Fig 4.** One dimensional SAXS profile of MNPs $Fe_3O_4$ as a function of pH fitted by combining two model calculations in a different region, log-normal sphere and mass fractal

**Table 1.** The particle diameter of magnetic nanoparticles with pH variation, Hydrodynamic diameters ($d_H$, nm), size of fractal aggregate (ξ, nm)

| pH samples | Size (nm) | | PdI |
|---|---|---|---|
| | $d_H$ | ξ | |
| 2 | 21 | 21 | 0.2 |
| 3 | 25 | 24 | 0.2 |
| 4 | 35 | 33 | 0.3 |
| 5 | 165 | 103 | 0.6 |

The DLS result confirms the appearance of aggregates measured using the SAXS technique, then the presumption of hierarchical structures of MNPs $Fe_3O_4$ can be verified. Even though the primary particles of aggregates could not be investigated through DLS measurement, the value of $d_H$ can be employed to be compared with the value of ξ from SAXS measurement.

Based on Derjaguin, Landau, Verwey, Overbeek (DLVO) theory, stability or instability of charged colloidal systems is influenced by competition between London-van der Waals forces of attraction and electrostatic forces of repulsion [14]. Due to the oxidation state of a metal oxide, iron oxide can form an amphoteric oxide with a pH-dependent surface [15]. This characteristic makes iron oxide's surface become positive in the acidic condition or at low pH and negative in the basic condition or at high pH. Theoretically, in an aqueous solution, iron oxide's surface properties will be altered to form surface hydroxyl groups (Fe–OH sites). Under this condition, the proton transfer could occur with surface protonation ($Fe-OH+H^+ \leftrightarrow Fe-OH_2^+$) and deprotonation ($Fe-OH \leftrightarrow Fe-O^- + H^+$) [16]. Therefore, at the low pH condition, the surface of iron oxide particles was positive charged due to protonation reaction ($Fe-OH_2^+$). The surface charge will generate electrostatic forces of repulsion and decrease the aggregation of particles.

As the result of SAXS measurement, we found that the hierarchical structure of fractal aggregate reflected the aggregation phenomenon as the function of pH solution. The increasing of pH solution will increase the fractal size, which means that the amphoteric surface of MNPs $Fe_3O_4$ can control the aggregation of particles.

Table 1 shows the pH-dependent of iron oxide influence the aggregation particles. At pH 2, the measurement using DLS technique resulted in $d_H$ ca. 21 nm, while the SAXS measurement resulted ξ ca. 21 nm. These sizes increase with the increase of pH until pH 5 with $d_H$ ca. 165 nm and ξ ca. 103 nm. This condition proved that the surface charge particles become stronger at low pH, and the electrostatic repulsion forces become higher. These phenomena will decrease the aggregation of particles and formed smaller size of aggregates. The surface charge and electrostatic stability reach a minimum point at isoelectric point or point of zero charges (PZC) with pH = PZC = 7.4. If the pH is closer to the PZC, so the tendency of magnetic nanoparticles forming the aggregate is higher [16].

The existence of a larger aggregate size at a higher pH value can be explained as the charge neutralization phenomenon [17-18]. As explained before, the MNPs $Fe_3O_4$ are highly positively charged in low pH, and with the increasing of pH the positive charge will decrease until the point of zero charges. The positive charge on

particles' surface will enhance the electrostatic forces of repulsion among particles and decrease the aggregation. While the increase of the pH solution will reduce the positive charge, and as a result, the aggregate will become larger due to the decreasing of electrostatic forces of repulsion among the particles.

Concerning aggregation, there is a correlation between polydispersity and aggregation particles. Aggregation alters the magnetic nanoparticle's size distribution. The increasing aggregation effect on magnetic nanoparticles will increase particles' size distribution, which can be seen as log-normal distribution on scattering data analysis.

The standard deviation of particle size distribution gives important information about the width of the distribution. Log-normal distribution has an asymmetrical curve, skewed with low mean values, variances large and positive values, see Fig. 5. Generally, distribution appears with a symmetrical curve called normal distribution, which can easily be characterized and described by additive calculation of mean and standard deviation. On the other hand, the log-normal distribution has a different kind of calculation called multiplicative, which is the log-transformed variable mean and standard deviation model.

Galton has described particle distribution range with multiplying and dividing ($^{x}$/ or times/divide) [19]. Concerning this experimental result using log-normal distribution, the range of particle size is $6.68^{x}$/3.16 or 2.11–21.10 nm.

The mechanism of aggregate formation influences the dimension of fractal objects. The aggregates fractal dimension determined in this work indicated that a reaction-limited cluster aggregation (RLCA) mechanism occurred in the magnetic nanoparticles system [20]. In this mechanism, particles' collisions formed a more compact aggregate due to the slow diffusion of particles into the center of aggregate. A sheet-like aggregate would have a fractal dimension closer to two.

The illustration model of aggregate fractal or primary particles formed a building block is shown in Fig. 6. The two fractal dimensions indicate correlations between points on each particle forming a single cluster.

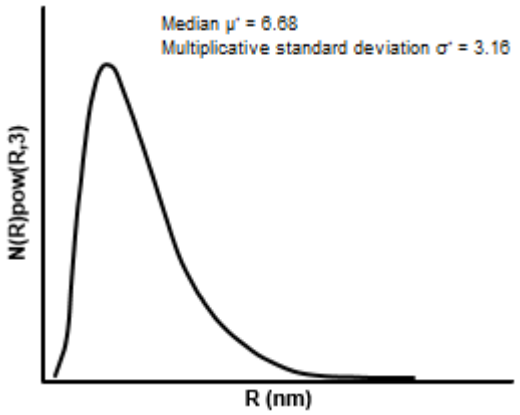


**Fig 5.** Log-normal distribution fitted to the experimental data ferrofluids

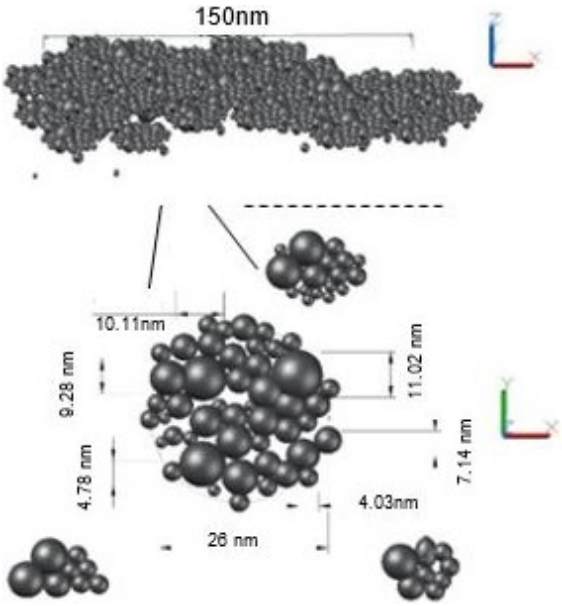


**Fig 6.** The illustration model presenting fractal objects of magnetic nanoparticle

The single cluster then interacted with each other to form a 2-dimensional fractal aggregate with a sheet-like structure.

Moreover, as the overall result of this experiment, it can be confirmed that the hierarchical structures of materials can be investigated using the SAXS technique. In contrast, DLS measurement is not able to provide information related to those structures. The primary particle with the size of 2 nm in a radius resulting from SAXS measurement is important information to be investigated. The other techniques measure the overall aggregate size.

## ■ CONCLUSION

The structure of a series of magnetic nanoparticles $Fe_3O_4$ or ferrofluid as pH variation has been successfully characterized using Small Angle X-ray Scattering (SAXS). The fitting analysis of the scattering pattern of ferrofluids was conducted by applying global fitting with the combination of a log-normal sphere and mass fractal models. It confirmed that the hierarchical structures containing primary particles and fractal aggregate of MNP $Fe_3O_4$ can be investigated using SAXS measurement. The aggregates have a similar particle size of 2 nm in radius with the particle size distribution of 0.5 for all the pH variations, then the size of fractal aggregate from ca. 21 nm to 103 nm in diameter for the pH of 2, 3, 4 and 5, respectively. The log-normal sphere and the mass fractal model calculations have high suitability fitted to SAXS data of ferrofluids

## ■ ACKNOWLEDGMENTS

This work was supported partially by the Synchrotron Light Research Institute of Thailand (SLRI–Thailand) and the Centre for Science and Technology of Advanced Materials–BATAN. The authors were also appreciative of the Polytechnic Institute of Nuclear Technology for providing a research grant Reg. No. 69/STTN/VI/2018 to support this work.

## ■ REFERENCES

[1] Wu, Y., Yang, X., Yi, X., Liu, Y., Chen, Y., Liu, G., and Li, R., 2015, Magnetic nanoparticles for biomedicine applications, *J. Nanotechnol. Nanomed. Nanobiotechnol.*, 2, 003.

[2] Engelmann, U., Buhl, E.M., Baumann, M., Schmitz-Rode, T., and Slabu, I., 2017, Agglomeration of magnetic nanoparticles and its effects on magnetic hyperthermia, *Curr. Dir. Biomed. Eng.*, 3 (2), 457–460.

[3] Chu, X., Yu, J., and Hou, Y.L., 2015, Surface modification of magnetic nanoparticles in biomedicine, *Chin. Phys. B*, 24 (1), 014704.

[4] Rodriguez, A.F.R., Rocha, C.O., Piazza, R.D., dos Santos, C.C., Morales, M.A., Faria, F.S.E.D.V., Iqbal, M.Z., Barbosa, L., Chaves, Y.O., Mariuba, L.A., Jafelicci, M., and Marques, R.F.C., 2018, Synthesis, characterization, and applications of maghemite beads functionalized with rabbit antibodies, *Nanotechnology*, 29 (36), 365701.

[5] Sulungbudi, G.T., Yuliani, Lubis, W.Z., Sugiarti, S., and Mujamilah, 2017, Controlled growth of iron oxide magnetic nanoparticles via co-precipitation method and $NaNO_3$ addition, *JUSAMI*, 18 (3), 136–143.

[6] Anitas, E.M., 2015, Fractal fragmentation and small angle scattering, *J. Phys. Conf. Ser.*, 633, 012119.

[7] Anitas, E.M., 2017, "Small-angle scattering from mass and surface fractals" in *Complexity in Biological and Physical Systems – Bifurcations, Solitons and Fractals*, Eds. Lopez-Ruiz, R., IntechOpen, London, United Kingdom.

[8] Taufiq, A., Sunaryono, Hidayat, N., Hidayat, A., Putra, E.G.R., Okazawa, A., Watanabe, I., Kojima, N., Pratapa, S., and Darminto, 2017, Studies on nanostructure and magnetic behaviors of Mn-doped black iron oxide magnetic fluids synthesized from iron sand, *Nano*, 12 (9), 1750110.

[9] Putra, E.G.R., Seong, B.S., Shin, E., Ikram, A., Ani, S.A., and Darminto, 2010, Fractal structures on $Fe_3O_4$ ferrofluid: A small-angle neutron scattering study, *J. Phys. Conf. Ser.*, 247, 012028.

[10] Rugmai, S., and Soontaranon, S., 2013, *Manual for SAXS/WAXS data processing using SAXSIT*, https://www.slri.or.th/en/bl13w-saxs.html.

[11] Kohlbrecher, J., and Bressler, I., 2011, *Software package SASfit for fitting small-angle scattering curve*, Laboratory for Neutron Scattering, Paul Scherrer Institut, Switzerland.

[12] Londoño, O.M., Tancredi, P., Rivas, P., Muraca, D., Socolovsky, L.M., and Knobel, M., 2018, "Small angle X-ray scattering to analyze the morphological properties of nanoparticulated systems, in *Handbook of Materials Characterization*, Eds. Sharma, S., Springer, Cham, Switzerland.

[13] Teixeira, J., 1988, Small-angle scattering by fractal systems, *J. Appl. Crystallogr.*, 21 (6), 781–785.

[14] Choi, Y.W., Lee, H., Song, Y., and Sohn, D., 2015, Colloidal stability of iron oxide nanoparticles with

multivalent polymer surfactants, *J. Colloid Interface Sci.*, 443, 8–12.

[15] Meng, X., Ryu, J., Kim, B., and Ko, S., 2016, Application of iron oxide as a pH-dependent indicator for improving the nutritional quality, *Clin. Nutr. Res.*, 5 (3), 172–179.

[16] Pfeiffer, C., Rehbock, C., Hühn, D., Carrillo-Carrion, C., de Aberasturi, D.J., Merk, V., Barcikowski, S., and Parak, W.J., 2014, Interaction of colloidal nanoparticles with their local environment: The (ionic) nanoenvironment around nanoparticles is different from bulk and determines the physico-chemical properties of nanoparticles, *J. R. Soc. Interface*, 11 (96), 20130931.

[17] Cruz, D., Pimentel, M., Russo, A., and Cabral, W., 2020, Charge neutralization mechanism efficiency in water with high color turbidity ratio using aluminium sulfate and flocculation Index, *Water*, 12 (2), 572.

[18] Vereda, F., Martin-Molina, A., Hidalgo-Alvarez, R., and Quesada-Pérez, M., 2015, Specific ion effects on the electrokinetic properties of iron oxide nanoparticles: Experiments and simulations, *Phys. Chem. Chem. Phys.*, 17 (26), 17069–17078.

[19] Limpert, E., Stahel, W.A., and Abbt, M., 2001, Log-normal distributions across the sciences: Keys and clues: On the charms of statistics, and how mechanical models resembling gambling machines offer a link to a handy way to characterize log-normal distributions, which can provide deeper insight into variability and probability—normal or log-normal: That is the question, *BioScience*, 51 (5), 341–352.

[20] Jungblut, S., Joswig, J.O., and Eychmüller, A., 2019, Diffusion- and reaction-limited cluster aggregation revisited, *Phys. Chem. Chem. Phys.*, 21 (10), 5723–5729.